npj Computational Materials

www.nature.com/npjcompumats

ARTICLE OPEN

Check for updates

First-principles search of hot superconductivity in La-*X*-H ternary hydrides

Simone Di Cataldo[1,2]✉, Wolfgang von der Linden[1] and Lilia Boeri[2,3]✉

Motivated by the recent claim of hot superconductivity with critical temperatures up to 550 K in La + *x* hydrides, we investigate the high-pressure phase diagram of compounds that may have formed in the experiment, using first-principles calculations for evolutionary crystal structure prediction and superconductivity. Starting from the hypothesis that the observed T_c may be realized by successive heating upon a pre-formed LaH_{10} phase, we examine plausible ternaries of lanthanum, hydrogen and other elements present in the diamond anvil cell: boron, nitrogen, carbon, platinum, gallium, gold. We find that only boron and, to a lesser extent, gallium form metastable superhydride-like structures that can host high-T_c superconductivity, but the predicted T_c's are incompatible with the experimental reports. Our results indicate that, while the claims of hot superconductivity should be reconsidered, it is very likely that unknown H-rich ternary or multinary phases containing lanthanum, hydrogen, and possibly boron or gallium may have formed under the reported experimental conditions, and that these may exhibit superconducting properties comparable, or even superior, to those of currently known hydrides.

npj Computational Materials (2022)8:2 ; https://doi.org/10.1038/s41524-021-00691-6

INTRODUCTION

Since the discovery of high-temperature superconductivity (HTSC) in compressed sulfur hydride in 2014[1,1,2], the race for HTSC has dramatically accelerated, leading to a *hydride rush* fueled by ab initio predictions.

As of 2020, all binary hydrides have been computationally explored[3–5], and many have been synthesized[6–12]. After LaH_{10} established the T_c record for binary hydrides in 2019, in 2020 Snider et al.[13] reported a T_c of 288 K in a compressed mixture of carbon, sulfur, and hydrogen, effectively realizing a room temperature superconductor. Compared to binary hydrides, ternary (or, in general, multinary) hydrides exhibit an increased chemical versatility, which may be exploited to tune the superconducting properties. Since Migdal–Eliashberg theory does not pose a hard limit to T_c, it is possible that multinary hydrides may exhibit superconductivity at sensibly higher T_cs than the known binaries; for example, T_c's largely exceeding room temperature have been predicted in a Li–Mg–H alloy[14].

In the summer of 2020, Grockowiak et al. reported experimental evidence of superconductivity with onset temperatures growing from 294 to 550 K upon successive heating cycles of a mixture of lanthanum and ammonia borane at about 180 GPa[15]. This may have been an experimental observation of hot superconductivity in a multinary hydride; unfortunately, due to COVID restrictions, the authors were able to report only partial evidences, and did not provide information on the chemical composition and structure of the superconducting samples, which would be fundamental for reproducibility. Even if one is skeptical about the highest values of T_c reported, it is possible that one or more multinary phases may have formed, calling for further studies.

In the absence of conclusive experimental information, such a question can effectively be addressed by first-principles methods for crystal structure prediction and superconductivity, which have demonstrated an extraordinary accuracy for binary hydrides[3–5,16].

In this paper, we perform an exploratory ab initio study of possible candidates for hot superconductivity, using evolutionary crystal structure prediction and linear-response calculations of the electron-phonon coupling. We explore all possible ternary combinations of lanthanum, hydrogen, and a third element present in the diamond anvil cell (DAC) in the experiment of ref. [15]: boron and nitrogen (from the hydrogen source), carbon, from the epoxy, platinum, gallium, and gold, from the electrical contacts. One (or more) of these elements may react with lanthanum and hydrogen to form an unknown superhydride. Our aim is to sample the ternary phase diagrams with an accuracy sufficient to estimate the probability that stable or weakly metastable structures may form at high pressure, determine the characteristic structural motifs, and assess their potential for high-T_c conventional superconductivity. We choose to carry out all of our structural searches at 300 GPa, rather than 180 GPa, which is the highest pressure measured in the experiment, and examine both the thermodynamically stable and metastable structures when scanning for potential superconductors, to expand the landscape of possible candidates[17]. In fact, there is rather extensive evidence that static Density Functional Theory (DFT) calculations, which neglect quantum lattice effects, tend to overestimate the stabilization pressure of hydrides[18,19] by as much as 100 GPa, and higher pressures typically yield better agreement with experiments also for superconducting properties. In addition, once we established that nitrogen and boron were the elements most likely to form a ternary superhydride, we performed additional searches for those elements at 150 GPa, to rule out the possibility of missing relevant phases.

We show that, among all elements present in the DAC, only nitrogen and boron form thermodynamically stable ternary structures with La and H, while the other elements do not form any stable ternary structure (Ga, Pt, C, Au); a few La–Ga–H hydrides are found very close to the convex hull, i.e. are likely metastable. Nitrogen forms stable and metastable structures that do not

[1]Institute of Theoretical and Computational Physics, Graz University of Technology, NAWI Graz, 8010 Graz, Austria. [2]Dipartimento di Fisica, Sapienza Università di Roma, 00185 Roma, Italy. [3]Centro Ricerche Enrico Fermi, Via Panisperna, 89a, 00184 Roma, Italy. ✉email: simone.dicataldo@uniroma1.it; lilia.boeri@uniroma1.it

Published in partnership with the Shanghai Institute of Ceramics of the Chinese Academy of Sciences

npj nature partner journals

exhibit the typical characteristics of high-T_c superhydrides: high-symmetry, large hydrogen content, large fraction of H states at the Fermi level. On the other hand, some stable and metastable La–B–H structures are characterized by the same hydrogen cage-like motifs encountered in many record superhydrides[20,21], and some metastable La–Ga–H structures present a similar dense hydrogen sublattice. In particular, within the limitations posed by the maximum cell size, our best superconducting phases are $LaBH_{17}$ and $LaGaH_{14}$, with a T_c of 180 and 137 K respectively, which are way too low to explain the hot superconductivity observed in ref. [15]. Tuning of the electronic and vibrational properties through doping or impurities may increase this value up to a factor two, but it is extremely unlikely that this type of structures may reach T_c's as high as 550 K.

This paper is organized as follows. The Results and Discussion section is further divided in the Phase diagrams subsection, where we discuss some general criteria leading to the formation of stable ternary phases, and present the predicted phase diagrams; In the Electronic properties subsection, where we analyze the electronic structure of the predicted phases; And in the Superconducting properties section, we discuss the superconducting properties of the metallic phases. The Methods section contains computational details on the structural searches and superconductivity calculations.

RESULTS AND DISCUSSION

Phase diagrams

Our structural searches were carried out using evolutionary algorithms as implemented in the Universal Structure Predictor: Evolutionary Xtallography (USPEX) code[22,23]. Further details on the structural searches can be found in the Computational Details section. Since full structural searches of ternary diagrams are extremely expensive computationally, before sampling in-depth the ternary compositions, we carried out a pre-screening process by first sampling roughly all possible combinations of elements, and then re-sampling those where stable compositions appeared.

The elements that we chose to analyze are based on a few considerations on the experimental report. According to the authors, the first onset of a superconducting transition occurred at 294 K (not far from the reported value for LaH_{10}), and T_c gradually shifted towards higher temperatures, upon further heating. It seems reasonable to assume that LaH_{10} was formed first, and, with the subsequent heating cycles, the sample underwent further structural transitions into an unknown multinary hydride phase, incorporating one or more of the elements present in the diamond anvil cell during the experiment. The diamond anvil cell was loaded with pure lanthanum and ammonia borane (NH_3BH_3), which acts both as a hydrogen source and as pressure medium, and the authors mention as possible contaminants also platinum, gallium, and gold from the electrodes, and carbon from the epoxy binder. In principle, any combination of these elements may be responsible for the observed hot superconductivity phase.

We calculated the ternary convex hulls for La–*X*–H structures (X = B, N, Ga, Pt, C, Au), sampling 3000 structures for each diagram. This search resulted in no stable (or weakly metastable) compositions for La–C–H, La–Au–H, and La–Pt–H, while several stable/metastable ones were already found for La–N–H, and La–B–H, and a few metastable ones—but none stable—were found for La–Ga–H.

This led us to dismiss further investigation of La–C–H, La–Au–H, and La–Pt–H, and to devote our resources to a better sampling of the others. In La–Ga–H we re-sampled the $(LaGa)_xH_{1-x}$ pseudo-binary, where the ternaries closest to the hull were present, to check whether any would become stable, but to no avail. Boron and nitrogen, on the other hand, were the most abundant elements other than hydrogen and lanthanum during the experiment, and thus are the most likely candidates to form ternary La–*X*–H hydrides. The existence of high-pressure compounds involving La, N, and B, as well as metal boron hydrides also supports this hypothesis[24–27].

Having decided to focus on La–N–H, La–B–H, we improved our structural searches by performing a second structural search, sampling a total of 5000 structures, which add to the previously sampled 3000. In addition, we performed structural searches along several pseudo-binary phases, bringing the total number of structures sampled to about 15000. In these refined searches, we sampled unit cells as large as 48 atoms. See the Computational Details section for more information.

In Fig. 1 we report the convex hulls for La–N–H, La–B–H, and La–Ga–H. The convex hulls for La–Pt–H, La–C–H and La–Au–H, where no stable or metastable compounds are found are shown in Supplementary Fig. 1.

The La–N–H convex hull contains four stable ternary phases: LaN_2H_3, LaN_3H_{10}, La_2N_2H, and La_4N_4H, as well as several metastable phases along the $(LaN)_xH_{1-x}$ line. We anticipate that none of the (meta)stable structures predicted in the La–N–H phase diagram is a likely candidate for HTCS since for most structures the hydrogen content is low, and H-rich weakly metastable structures are either low-symmetry or insulating.

In the La–B–H phase diagram we find three stable intermediate compositions: $LaBH_8$, $La_2B_6H_5$, and LaB_8H. In addition, several H-rich phases are predicted to be metastable (within 50 meV/atom from the hull, shown as red squares), suggesting that there is a strong tendency for La and B to form H-rich phases. While this work was under review, Liang et al. published a preprint with a thorough investigation of the ternary La–B-H phase diagram at 100, 150, 200, and 300 GPa[28]. In their work, the authors construct the convex hull by sampling the La_nB_m ($n = 1$, $m = 1$–6; $n = 2$, $m = 1$) pseudo-binaries, and predict the formation of the same $LaBH_8$ structure we report in our work.

In La–Ga–H phase diagram we could not find any stable ternary composition, but we do find a plethora of hydrogen-rich compositions close to the hull (i.e. within 50 meV/atom), indicating that metastable structures may in principle form. Among these, we analyzed three metastable structures with $LaGaH_6$, $LaGaH_{14}$, and $LaGaH_{15}$ composition, which were characterized by a more or less symmetric Bravais lattice (at least orthorhombic), and promising structural characteristics: high hydrogen fraction, and intermediate H–H distance. Since the formation of any of these phases is unlikely, in the following we only included the $LaGaH_{14}$ as representative of the La–Ga-H system. A discussion on the other phases can be found in the Supplemental Material.

In Fig. 2, we show the crystal structures of the stable La–N–H and La–B–H phases (the structure with LaN_3H_{10} composition is insulating, and is shown in Supplementary Fig. 3), together with two particularly significant metastable ones: $LaBH_{17}$ and $LaGaH_{14}$; additional information on the crystal structures with other elements, as well as all the structural data can be found in Supplementary Table 1 (The Supplemental Material is available at https://doi.org/10.1038/s41524-021-00691-6).

The La_4N_4H and La_2N_2H phases are characterized by a La–N sublattice with a cubic CsCl arrangement, in which hydrogen occupies the interstitial sites, with a H–H distance (d_{H-H}) of 3.6 and 2.6 Å, respectively. On the other hand, the LaN_2H_3 structure is characterized by the presence of La layers, alternated with a N–H network, and a H–H distance of 1.4 Å, while LaN_3H_{10} exhibits a disordered mixture of H_2 (d_{H-H} = 0.74 Å), NH, NH_2, and NH_3 molecules scattered around a La atom. The few metastable phases at high hydrogen content that we predict, are also characterized by the presence of disordered H_2 and NH_x molecules.

The LaB_8H phase exhibits a dense B–B network around each La atom, identical to the one predict for LaB_8, with hydrogen occupying interstitial positions between the second-nearest La–La atoms, with a H–H distance of 3.7 Å. The $La_2B_6H_5$ phase is characterized by the presence of two polymeric chains of BH_2 and B_2H_2, connected by a shared hydrogen atom, resulting in a H–H

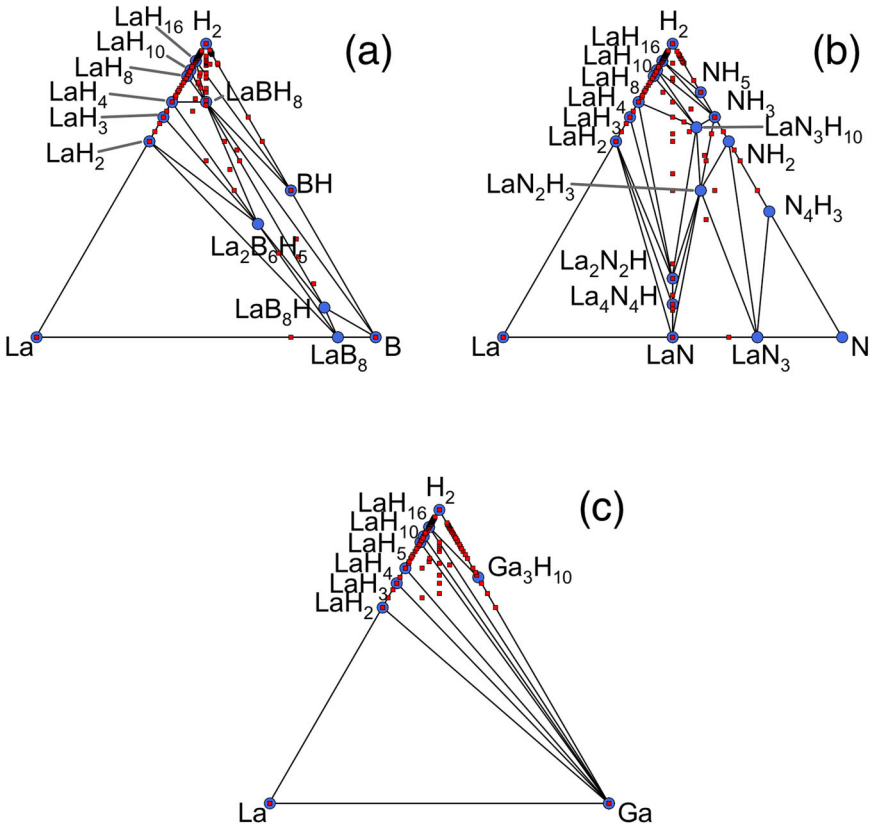

Fig. 1 Convex hulls for selected lanthanum ternary hydrides at 300 GPa. The convex hull shown are for La–N–H (**a**) and La–B-H (**b**), and La–Ga-H (**c**). Blue circles and red squares represent stable and metastable phases, respectively.

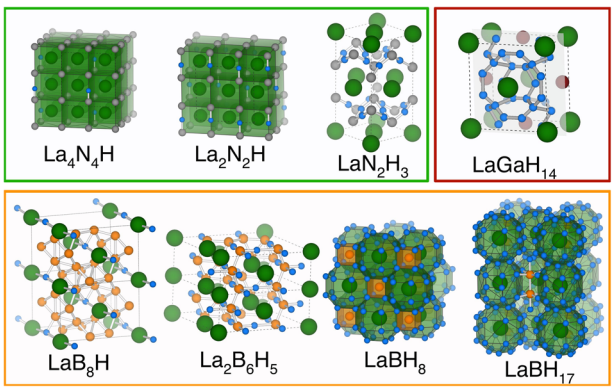

Fig. 2 Crystal structures of the thermodynamically stable La–B–H and La–N–H phases, and metastable $LaBH_{17}$ and $LaGaH_{14}$ phases. La, B, N, Ga and H atoms are shown as green, orange, gray, red, and blue spheres, respectively. Polyhedral surfaces match the color of the bonding atom. In $LaGaH_{14}$ the 001 lattice plane is shown to highlight the planar nature of the hydrogen network.

distance of 1.4 Å, while the La atom acts as a spacer among the polymers. The $LaBH_8$ phase exhibits a densely packed structure with two compenetrating face-centered cubic lattices for La and B, while H atoms form a rhombicuboctahedron around La and a cube around B. Nearest-neighboring hydrogen atoms form tetrahedra with a H–H distance of 1.33 Å. This phase is particularly interesting at lower pressures, as it remains stable down to 40 GPa, where it exhibits high-T_c superconductivity—further details have been discussed in ref. [26], while at 300 GPa the T_c is strongly suppressed by phonon hardening.

In the following we will focus on the crystal structure of $LaBH_{17}$ which, as we will discuss later on, exhibits the highest T_c among the structures examined. Its crystal structure presents a slightly distorted orthorhombic structure (α-$LaBH_{17}$), in which a cage of 32 H atoms surrounds a La atom. Neighboring cages are alternated with B_2H_{10} molecules. The cages are stacked along the vertical axis, sharing a slightly distorted hydrogen hexagon, with a H–H distance of 0.95 Å. At 500 GPa this phase undergoes a structural transition into a tetragonal structure (β-$LaBH_{17}$), which is essentially degenerate in energy with the orthorhombic one and only differs for a small rotation of the H cages with respect to the stacking axis and the regularization of the hydrogen hexagon. Most likely, the inclusion of quantum effects would remove the distortion at lower pressure, in the same way as reported for other superhydrides[18,19]. Both $LaBH_8$ and $LaBH_{17}$ have a relative hydrogen content above 50%, and are characterized by a symmetric lattice, with lanthanum and boron atoms encaged into hydrogen polyhedra, which form a sponge-like lattice, and hence are an example of a ternary hydride with a crystal structure that is reminiscent of sodalite clathrate hydrides.

The metastable $LaGaH_{14}$ structure is characterized by a base-centered orthorhombic La sublattice, interpenetrated by a simple orthorhombic Ga one. A dense planar hydrogen network is sandwiched between La–Ga planes, with a H–H distance ranging between 0.9 and 1.2 Å, quite similarly to the structure of $LaBH_{17}$. The structure of $LaGaH_{15}$ (Fig. S3) is also very similar.

Electronic properties

In Fig. 3, we report the total and atom-projected electronic Density of States (DOS) for the stable La–N–H and La–B-H phases, and metastable $LaBH_{17}$ and $LaGaH_{14}$. The structures for La_4N_4H and La_2N_2H are metallic and the partial DOS in the valence region is

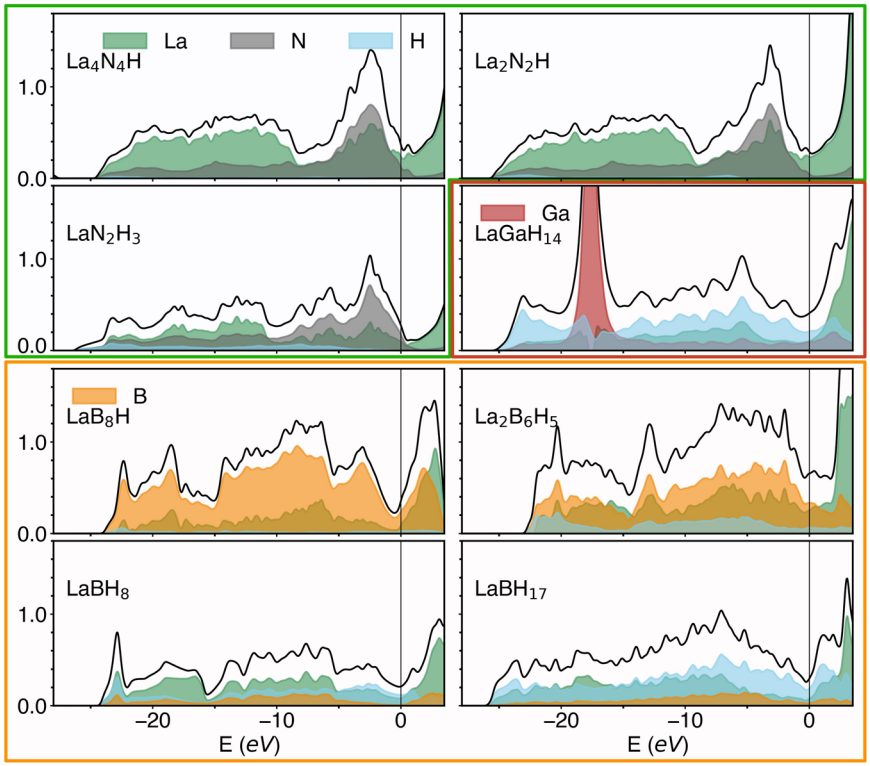

Fig. 3 Total and atom-projected DOS in units of $spin^{-1}eV^{-1}$ for stable La–N–H, La–B–H phases, and metastable $LaBH_{17}$ and $LaGaH_{14}$ at 300 GPa. The total DOS and its projection onto La, N, B, Ga, and H are shown as black lines, and green, gray, orange, red, and blue filled lines, respectively. The Fermi energy is set as the zero.

dominated by lanthanum and nitrogen, with little contribution from interstitial hydrogen. In LaN_2H_3 hydrogen gives a rather small contribution to the DOS from −25 to −5 eV, while nitrogen strongly contributes in the −10 to 0 eV range, and makes up most of the states at the Fermi level. LaN_3H_{10} (shown in Supplementary Fig. 6), on the other hand, is characterized by an insulating structure, with a band gap of 2.4 eV.

Overall, none of the La–N–H structures shown exhibit the typical characteristics of superconducting hydrides: high-symmetry structures, with high hydrogen content, and a large DOS at the Fermi level which is mostly derived from hydrogen. In La–N–H, we observe that at low concentration, hydrogen plays no significant role in the band structure near the Fermi energy, while at higher concentration, the structures formed are low-symmetry molecular crystals, either insulating, or with negligible contribution of hydrogen to the states near the Fermi energy.

The stable La–B–H structures (and metastable $LaBH_{17}$) are all metallic. In particular, LaB_8H is characterized by a partial DOS with a predominant boron contribution, while hydrogen contributes only very little. The $La_2B_6H_5$ structure exhibits a much larger, and rather constant, contribution of lanthanum to filled states. In both cases, however, hydrogen does not contribute significantly to the states at the Fermi level, nor does it play a significant role in the electronic structure. The structure for $LaBH_8$ is characterized by a partial DOS character rather equally distributed among La, B, and H in the −25 to −5 eV range, which gives way to a hydrogen-dominated DOS in the −5 to 1 eV range, including states at the Fermi level. Last, $LaBH_{17}$ exhibits a strong hydrogen character at all energies, as the structure is characterized by a weakly covalent hydrogen network, and a very high hydrogen concentration—The electronic band structures and Fermi surfaces of $LaBH_8$ and $LaBH_{17}$ are reported in Figs. S4 and S5. $LaBH_8$ and $LaBH_{17}$ are the only compositions for which the electronic structures are similar to the ones reported for sodalite-like superhydrides, i.e., a large hydrogen fraction of the states at the Fermi level $N_H/N(E_F)$, as well as a large overall DOS at the Fermi level ($N(E_F)$). Moreover, the structures of both $LaBH_8$ and $LaBH_{17}$ also satisfy a geometrical prerequisite: it was observed that the presence of weakly covalent hydrogen–hydrogen bonds positively correlates with T_c[29]. These bonds are associated with a H–H distance larger than 0.80 Å (i.e. no H_2 molecules), but smaller than 2 Å (i.e., significant H–H interaction). When the H–H interatomic distance satisfies these constraints the H lattice is so dense that a quasi-free electron gas is realized[30,31]. A possible descriptor to characterize the nature of the H–H bond in hydrides, called *connectivity*, was recently proposed by Belli et al.[29]. The connectivity value ϕ represents the highest value of the Electron Localization Function (ELF) for which the isocontour spans the cell without discontinuities in all directions. In particular, isolated high ELF regions surrounding H–H bonds are associated with molecular hydrogen, while a ϕ between approximately 0.4 and 0.8 is considered an indication of weak covalent bonds. For $LaBH_8$ and $LaBH_{17}$ at 300 GPa we find a connectivity value ϕ of 0.33 and, 0.43, respectively and no molecular bonds, which classifies $LaBH_{17}$, and possibly also $LaBH_8$, as a weak covalent hydride. For $LaGaH_{14}$ we find $\phi = 0.35$, placing it in the same ballpark as $LaBH_8$ and $LaBH_{17}$. The ELF corresponding to the ϕ value for the two La–B–H structures is shown in Fig. S7. The electronic properties of the structures of other metastable hydrides are shown in Fig. S4.

The $LaGaH_{14}$ structure is characterized by a large contribution of hydrogen to all occupied states. The occupied Ga-*d* states appear as a narrow peak around −18 eV, which however does not exhibit signs of hybridization with hydrogen or lanthanum, which instead occurs between −15 and 0 eV, as suggested by the three very similar projected DOS's. The DOS at the Fermi level, however, is characterized by a strong hydrogen character, around 60%, indicating that the hydrogen covalent sublattice is metallic.

Table 1. Electronic and superconducting properties of selected ternary phases of La–N–H and La–B–H, plus high-symmetry metastable La–Ga–H structures.

Composition	Space group	P (GPa)	ΔH (meV/atom)	d_{H-H} (Å)	$N(E_F)$ (10^3spin^{-1}eV^{-1}Å^{-3})	$N_H/N(E_F)$	λ	ω_{log} (K)	T_c^{ME} (K)
La_4N_4H	38	300	0	3.6	16.9	1%	0.24	434	0
La_2N_2H	63	300	0	2.6	4.2	3%	0.15	719	0
LaN_2H_3	66	300	0	1.4	10.3	1%	0.33	966	1
LaN_3H_{10}	1	300	0	0.74	–	–	–		–
LaB_8H	5	300	0	3.7	8.3	4%	0.44	973	8
$La_2B_6H_5$	8	300	0	1.5	12.0	21%	0.47	998	6
$LaBH_8$	225	300	0	1.33	7.4	62%	0.53	1731	14
α-$LaBH_{17}$	23	300	+33	0.95	7.8	63%	3.3	414	180
β-$LaBH_{17}$	97[a]	300	+33	0.96	7.9	64%	2.3[b]	759	179
LaH_{10}	225	300	0	1.06–1.14	16.4	62%	1.9	1575	249
$LaGaH_6$	71	300	+12	1.13	6.0	20%	0.63	845	21
$LaGaH_{14}$	35	300	+13	0.89–1.17	10.5	52%	1.25	1134	137
$LaGaH_{15}$	44	300	+11	0.90–1.10	11.7	57%	0.90	1338	95

The first column shows the composition, the second column indicates the space group. The fourth column ΔH indicates the enthalpy difference from the convex hull (0 if the structure is on the hull). d_{H-H} indicates the average H–H distance in Ångstrom. In the sixth and seventh column the electronic DOS at the Fermi level $N(E_F)$ and its relative hydrogen character are reported. The DOS is shown in units of 10^3spin^{-1}eV^{-1}Å^{-3} to allow for comparison between different pressures. The electron-phonon coupling coefficient λ and the average phonon frequency ω_{log} are defined in the Supplemental Material. The superconducting critical temperature T_c^{ME} was calculated by solving the isotropic Migdal–Eliashberg equations—for details see the Supplemental Material. [a]The structure is dynamically unstable near the M point. [b]cutting imaginary frequencies.

Superconducting properties

In order to asses whether there is a hot superconductor among the predicted structures, we calculated their vibrational and superconducting properties using Density Functional Perturbation Theory (DFPT). In addition to all stable La–N–H and La–B–H structures, we also included metastable ones from the other convex hulls if they respected the following criteria: (i) hydrogen content above 60%, (ii) symmetric lattice (at least orthorhombic), (iii) intermediate hydrogen–hydrogen distance (above 0.85 Å). Phonon frequencies were computed at the harmonic level, and the superconducting T_c due to $e-ph$ interaction was calculated by numerically solving the T-dependent isotropic Migdal–Eliashberg equations, using a standard value of μ^* of 0.10[32,33]. Our estimates do not take into account anharmonicity, whose effect should be to make our structures stable at lower pressures than the nominal harmonic instability pressure[6,18,34].

A summary of the electronic and vibrational properties of the stable phases of La–B–H and La–N–H, and of selected La–Ga–H and La–Pt–H phases at 300 GPa is reported in Table 1. All structures are dynamically stable, and the predicted T_c's are 8 K in LaB_8H, 6 K in $La_2B_6H_5$, 14 K in $LaBH_8$ and 180 K in $LaBH_{17}$, while La_4N_4H, La_2N_2H, and LaN_2H_3 exhibit a T_c below 1 K. Among the La–Ga–H and La–Pt–H metastable structures we find a few superconductors, and the highest T_c is found in $LaGaH_{14}$, with 137 K. As expected, the highest T_cs are observed for the structures with the highest hydrogen content. The similarities between La–B and La–Ga hydrides, which are the only systems where high-T_c superconductivity are not surprising. In fact, gallium and boron both belong to the 13th group. This result suggests that, in combination with lanthanum, metalloids and other post-transition metals should favor the formation of ternaries with superconducting properties, whereas halogens and other nonmetals have the tendency to suppress it.

In Fig. 4, we report the total and the atom-projected Éliashberg functions for all stable structures (except LaN_3H_{10}, which is insulating), as well as for metastable $LaGaH_{14}$ and $LaBH_{17}$. As shown in the figure, in both La_4N_4H and La_2N_2H it is mostly nitrogen vibrations which contribute to the overall $e-ph$ coupling, which is extremely small. In La_4N_4H, the H-derived modes with frequencies above 150 meV are absent, while they are present, albeit very weakly coupled, in La_2N_2H. It is clear that in these two structures hydrogen, which occupies the interstitial sites, does not play a significant role in the bonding or in the properties, and thus cannot contribute to the coupling. The spectrum of LaN_2H_3 is characterized by a few narrow peaks between 100 and 250 meV, with strong hydrogen character.

In LaB_8H the vibrational spectrum is dominated by boron, while in $La_2B_6H_5$ about 30% of it is hydrogen. In both cases however, the integrated $e-ph$ coupling λ is around 0.5, i.e. too low to lead to an appreciable T_c. In these cases the hydrogen content is rather low, therefore it is the B–B covalent bonding that dominates.

$LaBH_8$ and $LaBH_{17}$ are significantly different from LaB_8H and $La_2B_6H_5$: here essentially all of the coupling is concentrated into hydrogen modes. In particular, in $LaBH_8$ the coupling largely comes from modes around 170 meV, yielding a high ω_{log} of 135 meV, and a relatively low $\lambda = 0.5$. $LaBH_{17}$, on the other hand, exhibits a large value of the Eliashberg function at all energy ranges, concentrated on hydrogen modes. At 300 GPa, α-$LaBH_{17}$ is on the verge of a structural instability, as witnessed by its small ω_{log}, and large electron-phonon coupling constant $\lambda = 3.3$. At higher pressures the phonon harden. Both $LaBH_8$, $LaBH_{17}$, and $LaGaH_{14}$ exhibit the typical characteristic of high-T_c superhydrides, i.e., the presence of an interconnected, metallic hydrogen sublattice, which is manifested both in the large fraction of hydrogen states in the DOS at the Fermi level, and in a rather uniform distribution of the electron-phonon coupling over all phonon modes, as observed in binary high-T_c sodalite-like hydrides.

In another publication, we studied the superconducting behavior of $LaBH_8$ as a function of pressure in greater detail[35]. This structure remains dynamically stable down to 40 GPa, where the phonon modes are softer, and the T_c reaches 126 K. At 300 GPa however, the pressure-induced hardening of the phonon modes is so strong that suppresses the high-T_c.

The Éliashberg function for $LaGaH_{14}$, similarly to $LaBH_{17}$, is completely dominated by hydrogen, which constitutes 99% of its

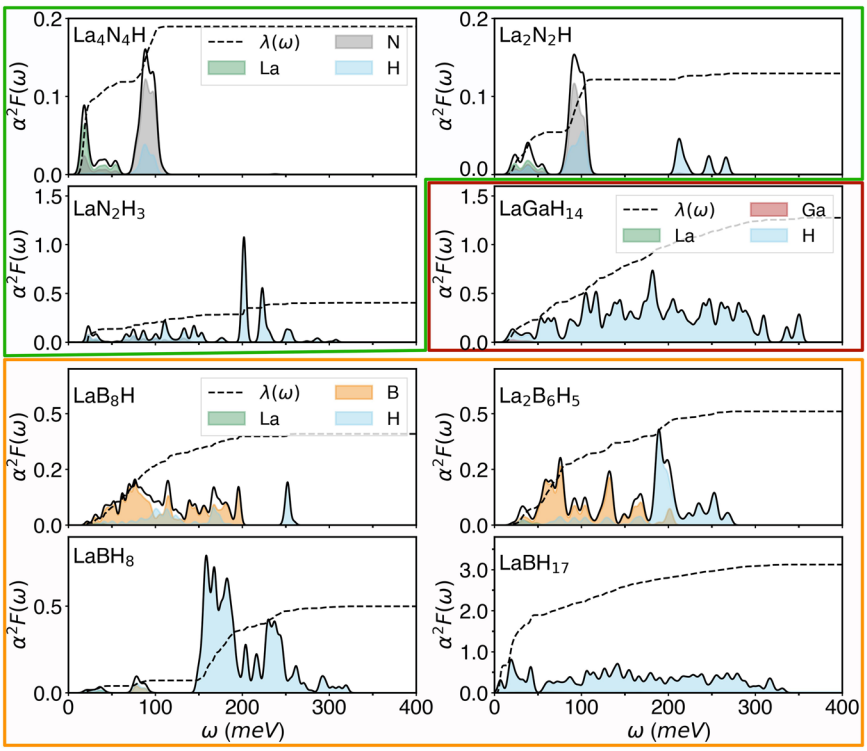

Fig. 4 Total and atom-projected Eliashberg function [$\alpha^2F(\omega)$, solid lines], and ω-dependent *e-ph* coupling [$\lambda(\omega)$, dashed lines] for stable La–B–H and La–N–H hydrides, and metastable $LaGaH_{14}$ and $LaBH_{17}$. The atom projections on La, B, N, Ga, and H are shown in green, gray, orange, red, and blue, respectively. The Eliashberg function and ω-dependent *e-ph* coupling $\lambda(\omega)$ are defined in Supplemental Material. Note: due to the large differences in values, the *y*-axis scale is different for each subfigure.

spectral weight. The coupling is evenly spread over all modes from 30 to 300 meV, which all contribute significantly to the total coupling λ, supporting the idea that superconductivity originates from the hydrogen sublattice only, and not from a specific, strongly coupled mode.

All other La–N–H and La–B–H structures are undoubtedly not superhydrides, and given their small hydrogen fraction it is not surprising that they are not high-T_c superconductors.

To rule out that the discrepancy between predicted T_c and experiments may be due to the pressure shift introduced to empirically take into account the effect of quantum lattice fluctuations we recomputed the critical temperatures of $LaBH_8$ and $LaBH_{17}$ also at 150 GPa, i.e. below the maximum pressure reported in experiments. Here, $LaBH_8$ is dynamically stable, with a T_c of 40 K, while $LaBH_{17}$ has a weak dynamical instability; neglecting imaginary frequencies, the predicted T_c is 223 K, i.e. well below 550 K. We also performed a structural search at 150 GPa for the La–B–H and La–N–H systems, but could not find any other potential hot superconductor.

We can also estimate, albeit in a rather qualitative fashion, the effect of possible mechanisms that may positively influence the T_c of related ternary and multinary La–B–H phases. An obvious observation is that the Fermi energy in $LaBH_{17}$ lies exactly in correspondence of a pseudogap. Carbon substitution at the boron site could sensibly enhance the T_c through charge doping; for example, a 50% replacement of boron with carbon would increase the DOS at the Fermi level by approximately a factor of two, and boost the T_c to about 290 K. If we assume that the Eliashberg function is rigidly multiplied by a factor equal to the increase in the DOS, in order to achieve 550 K one would need approximately an eight times larger DOS in $LaBH_8$, and a four times larger DOS at the Fermi level in $LaBH_{17}$. At most, a 100% substitution of boron with carbon would shift the Fermi energy enough to boost the DOS by a factor of two and a half, and the T_c to about 310 K, i.e. above room temperature, but well below 550 K.

Another possibility is to consider phases with a higher H content than $LaBH_{17}$; the shape of the La–B-H ternary hull gave strong indications that they may form. In this case, one may speculate that average phonon frequencies may be increased compared to $LaBH_{17}$, leading to an effective boost in T_c. However, even a doubling of all phonon frequencies of $LaBH_{17}$, which is extremely unlikely, would be sufficient to bring the T_c *only* to 360 K. Similar arguments also apply for $LaGaH_{14}$, as its Fermi energy is also situated in a pseudogap, and could be electron-doped via substitution of gallium with germanium, increasing the DOS at the Fermi level. However, even in the most optimistic scenario it would not be possible to reach the reported 550 K.

Outlook

In summary, following a recent experimental report of hot superconductivity at 550 K in a material with undetermined composition and structure[15], we investigated from first-principles the high-pressure phase diagram of the most likely combinations of elements which could have formed, i.e. La–*X*–H ternary hydrides (X = B, N, Pt, Au, Ga, C), looking for a candidate to explain the experimental results. The choice of La-based ternary hydrides is motivated by the T_c measured after the first heating cycle, which is compatible with that of LaH_{10}. As *X* element we considered all the elements that were reported to be present in the diamond anvil cell during the experiment: boron, nitrogen, hydrogen, and traces of platinum, gold, gallium and carbon.

In order to evaluate which ternary hydrides are thermodynamically favorable, we used variable-composition, evolutionary algorithms, at increasing levels of accuracy. According to our calculations, only La–N–H and La–B–H can form stable ternary phases, but formation of metastable La–Ga–H hydrides may be possible. Only in La–B–H and La–Ga-H do we predict the formation of H-rich, highly symmetric

structures, which can host high-T_c superconductivity. In particular, we identified a high-T_c tetragonal $LaBH_{17}$ phase, characterized by a dense hydrogen sublattice which is reminiscent of other high-T_c binary sodalite-like hydrides. For this structure we predicted a T_c of 180 K at 300 GPa by numerically solving the isotropic Migdal–Eliashberg equations. This result is way too far from the reported value of hot superconductivity to attribute the difference to numerical errors, and even within the most optimistic doping scenarios we could not increase T_c above 360 K. The discrepancy is too large for anharmonic lattice effects to affect our main conclusions.

While none of the binary or ternary phases of the elements considered in this work can explain the extreme T_cs reported, the La–B–H and La–Ga–H systems represent a very interesting starting point for further superconductivity studies. In fact, the extreme complexity of a ternary search limited our calculations in the maximum size of the unit cell, and the extent of the sampling for each composition, but our calculations suggest that the formation of high-H content La–B–H phases, or even quaternary phases involving lanthanum, hydrogen, and boron, nitrogen or gallium, with high T_c is definitely possible. Therefore, we urge the authors of ref. [15] to repeat their experiments under controlled conditions; it would be interesting, for example, to repeat the experiments employing diborane (B_2H_6), instead of ammonia borane as a hydrogen source, to discriminate between purely ternary La–B–H phases and quaternary La–B–N–H ones, or to intentionally include a larger amount of gallium in the cell.

We hope that a more precise determination of the critical temperature and a clearer indication of the elements and crystal structures will help elucidate the fascinating high-pressure physics of these systems.

Note: While this work was under review, we became aware of two other studies involving the La–B–H system[28,36].

METHODS

Structure search

To construct the phase diagrams, variable-composition structural searches were carried out using evolutionary algorithms as implemented in the USPEX software[22,23]. During the structural search, every structure was relaxed using a five-step process to minimize stress and forces, calculated within DFT. These calculations were performed using the Vienna ab initio Software Package[37], using projector augmented waves pseudopotentials with Perdew–Burke–Ernzerhof exchange-correlation functional. We used a progressively tighter convergence, up to a cutoff on the plane waves expansion of 600 eV; a regular grid in $\vec{k}$ space with a 0.04 spacing in units of $\frac{2\pi}{\text{Å}}$, and a Methfessel–Paxton smearing with a width of 0.03 eV for reciprocal-space integration. The validity of the pseudopotentials was subject to an internal consistency check, as electronic structure and superconductivity calculations were carried out using Quantum ESPRESSO (QE) with Norm-Conserving pseudopotentials (see next Section). Therefore all the structures examined were re-relaxed using QE, with a different pseudopotential, and were always found to be already at the minimum.

The ternary hulls were constructed following a multi-step procedure similar to the one proposed in ref. [38]:

1. We performed a variable-composition evolutionary search with no restrictions, except for the maximum number of atoms in the unit cell, which was set to 20. For this search we considered 30 generations with 200 individuals in the first, and 60 individuals in each subsequent generation. While this level of accuracy is hardly enough to correctly identify the minima of the enthalpy for many compositions, it is sufficient to assess the possible formation of intermediate ternary phases.
2. We extended our search to binary phases on the edges of the ternary hull, and for selected pseudo-binaries, the latter with a larger unit cell (up to 40 atoms). The pseudo-binary phases which were re-sampled are: $(LaN)_xH_{1-x}$, $(LaN_2)_xH_{1-x}$, $(LaN_3)_xH_{1-x}$, $(LaH_{10})_x(NH_3)_{1-x}$, $(LaH_{10})_x(NH_5)_{1-x}$, $(LaH_{16})_x(NH_3)_{1-x}$, $(LaH_4)_x(NH_2)_{1-x}$, $(LaB)_xH_{1-x}$, $(LaB_3)_xH_{1-x}$, $(LaH_2)_x(BH)_{1-x}$, $(LaH_3)_x(BH)_{1-x}$, $(LaH_4)_x(BH)_{1-x}$, $(LaH_8)_x(BH)_{1-x}$, $(LaH_{10})_x(BH)_{1-x}$, $(LaH_{16})_x(BH)_{1-x}$, $(LaGa)_xH_{1-x}$, and $(LaPt)_xH_{1-x}$
3. **Only for La–N–H and La–B–H**. Motivated by the presence of stable ternary phases, we performed a final variable-composition evolutionary search, using all the stable structures found in the previous steps as seeds, with a maximum cell size of 40 atoms, a population size of 250 individuals, and 20 generations
4. All enthalpies at the previous steps were collected, and the convex hulls in Fig. 1 were constructed using `pymatgen`[39].

Where available, our convex hulls reproduce previous calculations for binary hydrides at comparable pressures[8,21,40–42].

The figures of the crystal structures were generated using VESTA[43].

Superconductivity

Calculations of electronic structure and electron-phonon properties were carried out in DFPT using QE[33,44–47] using Optimized Norm-conserving Vanderbilt Pseudopotentials (ONCV)[48]. A cutoff of 80 Ry was used for the plane-wave expansion of the wave functions. The boron–carbon virtual crystal pseudopotentials were generated by mixing the two ONCV pseudopotentials, using the tools provided within QE.

The structures were re-relaxed in QE until each component of the forces acting on single atoms was less than 2 meV/Å. Calculations of the ground-state charge density were carried out using a 0.04 Ry smearing and a $6\times6\times6$ grid in reciprocal space for $\vec{k}$ space integration. Phonon calculations were performed on a $4\times4\times4$ reciprocal-space grid for $LaBH_8$, and a $2\times2\times2$ grid for La_4N_4H, La_2N_2H, LaN_2H_3, LaB_8H, $La_2B_6H_5$, and a $3\times3\times3$ grid for $LaBH_{17}$, $LaGaH_6$, $LaGaH_{14}$, $LaGaH_{15}$, and $LaPtH_6$. The integration of the electron-phonon matrix elements on the Fermi surface was carried out using a $24\times24\times24$ $\vec{k}$ grid, and a gaussian smearing with a width of 200 meV to describe the zero-width limit of the electronic δ functions. The phonon DOS was obtained by performing Fourier interpolation on a $16\times16\times16$ $\vec{q}$ grid.

DATA AVAILABILITY

The authors declare that the data supporting the findings of this study are available within the paper and its Supplementary information files. The authors also declare their availability to provide additional data and information upon request.

Received: 14 June 2021; Accepted: 21 December 2021;
Published online: 10 January 2022

REFERENCES

1. Einaga, M. et al. Crystal structure of the superconducting phase of sulfur hydride. *Nat. Phys.* **12**, 835–838 (2016).
2. Duan, D. et al. Pressure-induced metallization of dense $(S_2H)_2H_2$ with high-T_c superconductivity. *Sci. Rep.* **4**, 6968 (2014).
3. Zurek, E. & Bi, T. High-temperature superconductivity in alkaline and rare-earth polyhydrides at high pressure: a theoretical perspective. *J. Chem. Phys.* **150**, 050901 (2019).
4. Flores-Livas, J. A. et al. A perspective on conventional high-temperature superconductors at high pressure: Methods and materials. *Phys. Rep.* **856**, 1–78 (2020).
5. Semenok, D. V., Kruglov, I. A., Savkin, I. A., Kvashin, A. G. & Oganov, A. R. On distribution of superconductivity in metal hydrides. *Curr. Opin. Solid State Mater. Sci.* **24**, 100808 (2020).
6. Drozdov, A. P. et al. Superconductivity at 250 K in lanthanum hydride under high pressure. *Nature* **569**, 528–531 (2019).
7. Somayazulu, M. et al. Evidence for superconductivity above 260 K in lanthanum superhydride at megabar pressures. *Phys. Rev. Lett.* **122**, 027001 (2019).
8. Liu, H., Naumov, I. I., Hoffmann, R., Ashcroft, N. W. & Hemley, R. J. Potential high-T_c superconducting lanthanum and yttrium hydrides at high pressure. *PNAS* **114**, 6990–6995 (2017).
9. Semenok, D. V. et al. Superconductivity at 161 K in thorium hydride thh_{10}: synthesis and properties. *Mat. Tod.* **33**, 36–44 (2020).
10. Troyan, I. A. et al. Anomalous high-temperature superconductivity in YH_6. *Adv. Mater.* **33**, 2006832 (2021).
11. Kong, P. P. et al. Superconductivity up to 243 K in yttrium hydrides under high pressure. Nat. Comm. 12, 5075 (2021).
12. Drozdov, A. P., Eremets, M. I. & Troyan, I. A. Superconductivity above 100 K in PH_3 at high pressures. Preprint at https://arxiv.org/abs/1508.06224 (2015).
13. Snider, E. et al. Room-temperature superconductivity in a carbonaceous sulfur hydride. *Nature* **586**, 373–377 (2020).

14. Sun, Y., Lv, J., Xie, Y., Liu, H. & Ma, Y. Route to a superconducting phase above room temperature in electron-doped hydride compounds under high pressure. *Phys. Rev. Lett.* **123**, 097001 (2019).
15. Grockowiak, A. D. et al. Hot hydride superconductivity above 550 K. Preprint at https://arxiv.org/abs/2006.03004 (2020).
16. Boeri, L. & Bachelet, G. B. Viewpoint: the road to room-temperature conventional superconductivity. *J. Phys.: Condens. Matter* **31**, 234002 (2019).
17. Shipley, A. M., Hutcheon, M. J., Needs, R. J. & Pickard, C. J. High-throughput discovery of high-temperature conventional superconductors. *Phys. Rev. B* **104**, 054501 (2021).
18. Errea, I. et al. Quantum hydrogen-bond symmetrization in the superconducting hydrogen sulfide system. *Nature* **532**, 81–84 (2016).
19. Errea, I. et al. Quantum crystal structure in the 250-Kelvin superconducting lanthanum hydride. *Nature* **578**, 66–69 (2020).
20. Zurek, E., Hoffmann, R., Ashcroft, N. W., Oganov, A. R. & Lyakhov, A. O. A little bit of lithium does a lot for hydrogen. *PNAS* **106**, 17640–17643 (2009).
21. Peng, F. et al. Hydrogen clathrate structures in rare earth hydrides at high pressures: possible route to room-temperature superconductivity. *Phys. Rev. Lett.* **119**, 107001 (2017).
22. Glass, C. W., Oganov, A. R. & Hansen, N. USPEX–evolutionary crystal structure prediction. *Comput. Phys. Commun.* **175**, 713–720 (2006).
23. Lyakhov, A. O., Oganov, A. R., Stokes, H. T. & Zhu, Q. New developments in evolutionary structure prediction algorithm uspex. *Comput. Phys. Commun.* **184**, 1172–1182 (2013).
24. Teredesai, P. et al. High pressure phase transition in metallic LaB_6: Raman and x-ray diffraction studies. Solid State Comm. 129 (2004).
25. Cava, R. J. et al. Superconductivity in lanthanum nickel boro-nitride. *Nature* **273**, 245–247 (1994).
26. Cataldo, S. D., von der Linden, W. & Boeri, L. Phase diagram and superconductivity of calcium borohydrides at extreme pressures. *Phys. Rev. B* **102**, 014516 (2020).
27. Kokail, C., von der Linden, W. & Boeri, L. Prediction of high-t_c conventional superconductivity in the ternary lithium borohydride system. *Phys. Rev. M* **1**, 074803 (2017).
28. Liang, X. et al. Prediction of high-T_c superconductivity in ternary lanthanum borohydrides. *Phys. Rev. B*, 134501 (2021).
29. Belli, F., Novoa, T., Contreras-Garcia, J. & Errea, I. Strong correlation between bonding network and critical temperature in hydrogen-based superconductors. *Nat. Commun.* **12**, 1–11 (2021).
30. Borinaga, M., Errea, I., Calandra, M., Mauri, F. & Bergara, A. Anharmonic effects in atomic hydrogen: Superconductivity and lattice dynamical stability. *Phys. Rev. B* **93**, 174308 (2016).
31. Azadi, S., Monserrat, B., Foulkes, W. M. C. & Needs, R. J. Dissociation of high-pressure solid molecular hydrogen: a quantum monte carlo and anharmonic vibrational study. *Phys. Rev. Lett.* **112**, 165501 (2014).
32. Allen, P. B. & Dynes, R. C. Transition temperature of strong-coupled superconductors reanalyzed. *Phys. Rev. B* **12**, 905 (1975).
33. Carbotte, J. P. Properties of boson-exchange superconductorsa. *Rev. Mod. Phys.* **62**, 1027 (1990).
34. Heil, C., Cataldo, S. D., Bachelet, G. B. & Boeri, L. Superconductivity in sodalite-like yttrium hydrides. *Phys. Rev. B* **99**, 220502(R) (2019).
35. Cataldo, S. D., Heil, C., von der Linden, W. & Boeri, L. $LaBH_8$: towards high-t_c low-pressure superconductivity in ternary superhydrides. *Phys. Rev. B* **104**, L020511 (2021).
36. Zhang, Z. et al. Design principles for high temperature superconductors with hydrogen-based alloy backbone at moderate pressure. Preprint at https://arxiv.org/abs/2106.09879 (2021).
37. Kresse, G. & Furthmüller, J. Efficient iterative schemes for ab-initio total-energy calculations using a plane-wave basis set. *Phys. Rev. B* **54**, 11169 (1996).
38. Kvashin, A. G., Tantardini, C., Zakaryan, H. A., Kvashina, Y. A. & Oganov, A. R. Computational search for new w-mo-b compounds. *Chem. Mater.* **32**, 7028–7035 (2020).
39. Ong, S. P. et al. Python materials genomics (pymatgen): a robust, open-source python library for materials analysis. *Comput. Mater. Sci.* **68**, 314–319 (2013).
40. Zhou, X.-F. et al. Superconducting high-pressure phase of platinum hydride from first principles. *Phys. Rev. B* **84**, 054543 (2011).
41. Hu, C.-H. et al. Pressure-induced stabilization and insulator-superconductor transition of BH. *Phys. Rev. Lett.* **110**, 165504 (2013).
42. Pickard, C. J. & Needs, R. J. Highly compressed ammonia forms an ionic crystal. *Nat. Mater.* 775–779 (2008).
43. Momma, K. & Izumi, F. Vesta: a three-dimensional visualization system for electronic and structural analysis. *J. Appl. Cryst.* **41**, 653–658 (2008).
44. Giannozzi, P. et al. Quantum espresso: a modular and open-source software project for quantum simulation of materials. *J. Phys. Condens. Matter* **21**, 395502 (2009).
45. Baroni, S., de Gironcoli, S., Corso, A. D. & Giannozzi, P. Phonons and related crystal properties from density-functional perturbation theory. *Rev. Mod. Phys.* **73**, 515 (2001).
46. Savrasov, S. Y. & Savrasov, D. Y. Electron-phonon interactions and related physical properties of metals from linear-response theory. *Phys. Rev. B* **54**, 16487 (1990).
47. Giannozzi, P. et al. Advanced capabilities for materials modelling with quantum espresso. *J. Phys. Condens. Matter* **29**, 465901 (2017).
48. Hamann, D. R. Optimized norm-conserving Vanderbilt pseudopotentials. *Phys. Rev. B* **88**, 085117 (2017).

ACKNOWLEDGEMENTS

We thank Antonio Sanna for kindly sharing with us the code for solving the isotropic Migdal–Eliashberg equations. The authors acknowledge computational resources from the dCluster of the Graz University of Technology and the VSC3 of the Vienna University of Technology, and support through the FWF, Austrian Science Fund, Project P30269-N36 (Superhydra). L.B. acknowledges funding through Progetto Ateneo Sapienza 2017-18-19 and computational Resources from CINECA, proj. Hi-TSEPH. S.D.C. acknowledges computational Resources from CINECA, proj. IsC90-HTS-TECH_C, and the dCluster of the Graz University of Technology.

AUTHOR CONTRIBUTIONS

S.D.C performed the calculations. W.v.d.L. and L.B. supervised the project. All authors analyzed the results and contributed to writing the manuscript.

COMPETING INTERESTS

The authors declare no competing interests.

ADDITIONAL INFORMATION

Supplementary information The online version contains supplementary material available at https://doi.org/10.1038/s41524-021-00691-6.

Correspondence and requests for materials should be addressed to SimoneDi Cataldo or Lilia Boeri.

Reprints and permission information is available at http://www.nature.com/reprints

Publisher's note Springer Nature remains neutral with regard to jurisdictional claims in published maps and institutional affiliations.